Progress In Electromagnetics Research Letters, Vol. 82, 129–137, 2019

Design of Dual/Tri-Band BPF with Controllable Bandwidth Based on a Quintuple-Mode Resonator

Sheng-Fang Zhang[1], Li-Tian Wang[1], Sheng-Hui Zhao[1], Jie Zhou[1], Zhi-Peng Wang[1], Xin Zhang[1], Xue-Lian Liang[1], Ming He[1, 2], and Lu Ji[1, 3, *]

Abstract—In this article, a new class of dual-/tri-band bandpass filters (BPFs) using a quintuple-mode resonator (QMR) is proposed. The classic odd-/even-mode analysis method is used to analyze the two filters due to their symmetrical structure. Owing to characteristics of the QMR, the dual-/tri-band BPFs based on the same topology are designed. The bandwidths (BWs) of the passbands are controllable. A dual-band BPF with center frequencies of 2.1 GHz/3.43 GHz and a tri-band BPF with center frequencies of 2.35 GHz/3.44 GHz/5.2 GHz are designed, fabricated, and measured. The fabricated filters are compact in size, and measured results are in good agreement with the simulated ones.

1. INTRODUCTION

With the rapid development of wireless communication systems, RF front-end devices, e.g., diplexer, low noise amplifier, and multi-band bandpass filter (BPF), are in great demand. As an important component of RF front-end devices, multi-band filters have attracted much attention. To meet the requirements of multi-band BPFs, two main methods have been used to design a BPF in reported works. The first method is to combine sets of resonators [1–7]. In [1, 3, 4], two resonators were used to design dual-band BPF or tri-band BPF. In [2], a dual-band BPF based on four half-wavelength resonators and four quarter-wavelength resonators was presented. Although [1, 2] have achieved bandwidth (BW) control, they suffered from large circuit size due to the number of the resonators. The second method is to use a multi-mode resonator [8–11]. A dual-band BPF using a quad-mode resonator was realized in [8] and [9]. In [10], the proposed tri-band BPF utilized a multi-stub-loaded resonator with eight resonant modes. In [11], a miniaturized tri-band BPF using a multi-mode stepped-impedance resonator was presented. Generally speaking, [11, 12] have smaller size than the filters combining sets of resonators, but the BW of the proposed filter could not be controlled. And some filters, such as filters in [9–11, 13–15], have difficulty in the fabrication due to some via holes or multi-layer structure. Hence, a multi-band BPF which has smaller size, controllable BW, and easier fabrication is worth studying.

In this article, a new class of dual-/tri-band BPFs based on a quintuple-mode resonator (QMR) is proposed, and the BWs of the two filters are controllable. It should be noticed that the BWs of the dual-band BPF can be controlled independently. By adjusting the electrical length and impedance, the dual-/tri-band BPFs based on the same topology are realized. Five transmission poles and three transmission zeros (TZs) are excited. The center frequencies of the two filters are located at 2.1 GHz/3.43 GHz and 2.35 GHz/3.44 GHz/5.2 GHz, respectively. By using the classic odd-/even-mode analysis method, features of the QMR are studied. For verification, the dual-/tri-band BPFs are fabricated and measured, and the measured results are consistent well with the simulated ones.

Received 13 November 2018, Accepted 13 January 2019, Scheduled 19 March 2019

* Corresponding author: Lu Ji (luji@nankai.edu.cn).

[1] College of Electronic Information and Optical Engineering, Nankai University, Tianjin 300350, China. [2] Tianjin Key Laboratory of Optoelectronic Sensor and Sensing Network Technology, Tianjin 300350, China. [3] Key Laboratory of Photoelectronic Thin Film Devices and Technology of Tianjin, Tianjin 300350, China.

2. CHARACTERISTICS OF THE PROPOSED QMR

Figure 1(a) shows an ideal transmission line model of the proposed filters. The proposed structure is symmetrical along the short-dashed-line. The characteristics of the symmetrical QMR will be analyzed by using odd-/even-mode analysis method. When the odd-mode is excited, the symmetrical plane is equivalent to an electric wall. When the even-mode is excited, the symmetrical plane is equivalent to a magnetic wall. Figure 1(b) and Figure 1(c) are the odd-mode equivalent circuit and even-mode equivalent circuit, respectively.

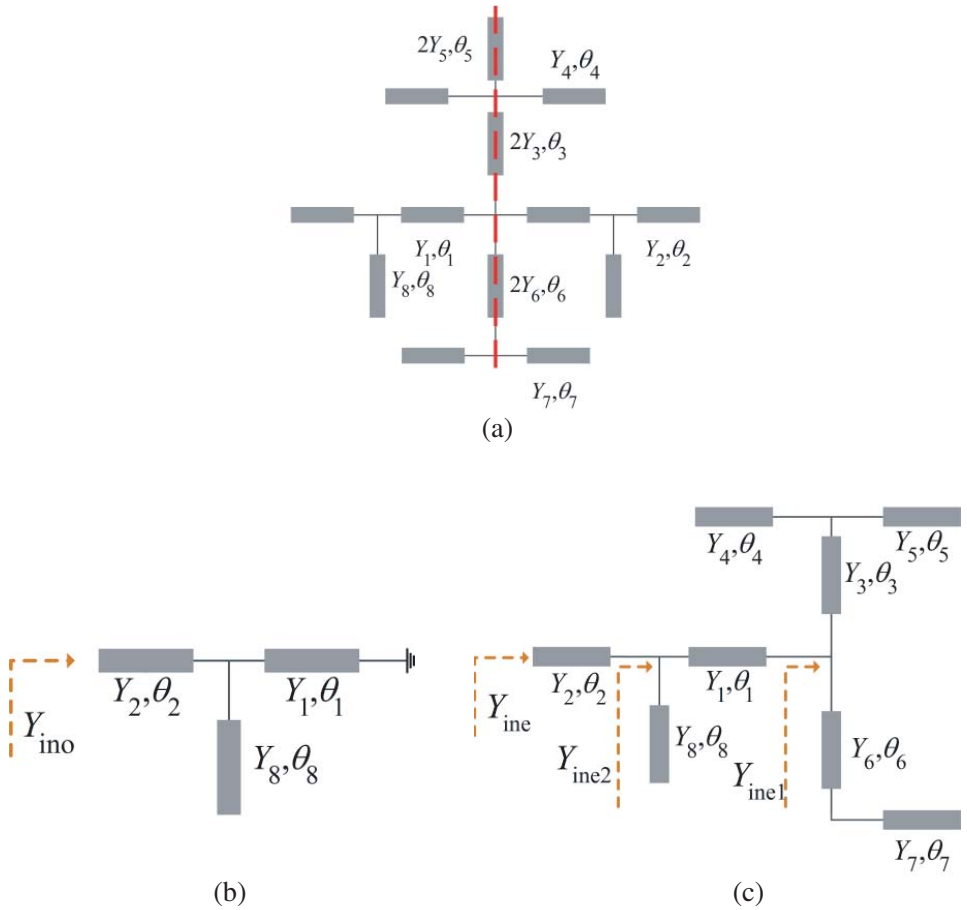

Figure 1. (a) Ideal transmission line model, (b) odd-mode equivalent circuit and (c) even-mode equivalent circuit of the QMR.

According to the resonant condition, the admittance in the case of odd-mode excitation can be written as

$$\mathrm{Im}(Y_{\mathrm{ino}}) = 0 \tag{1}$$

where,

$$Y_{\mathrm{ino}} = jY_2 \frac{Y_2 \tan\theta_2 + Y_8 \tan\theta_8 - Y_1 \cot\theta_1}{Y_2 - Y_8 \tan\theta_8 \tan\theta_2 + Y_1 \cot\theta_1 \tan\theta_2} \tag{2}$$

Similarly, the admittance in the case of even-mode excitation can be derived as

$$\mathrm{Im}(Y_{\mathrm{ine}}) = 0 \tag{3}$$

where,

$$Y_{\mathrm{ine}} = Y_2 \frac{Y_{\mathrm{ine2}} + jY_2 \tan\theta_2}{Y_2 + jY_{\mathrm{ine2}} \tan\theta_2} \tag{4}$$

$$Y_{\text{ine2}} = Y_1 \frac{Y_{\text{ine1}} + jY_1 \tan\theta_1}{Y_1 + jY_{\text{ine1}} \tan\theta_1} + jY_8 \tan\theta_8 \tag{5}$$

$$Y_{\text{ine1}} = jY_3 \frac{Y_3 \tan\theta_3 + Y_4 \tan\theta_4 + Y_5 \tan\theta_5}{Y_3 - Y_4 \tan\theta_4 \tan\theta_3 - Y_5 \tan\theta_5 \tan\theta_3} + jY_6 \frac{Y_6 \tan\theta_6 + Y_7 \tan\theta_7}{Y_6 - Y_7 \tan\theta_7 \tan\theta_6} \tag{6}$$

In this paper, $Y_n\,(n = 1, 2, \ldots, 8)$ denotes the characteristic admittances, and $\theta_n\,(n = 1, 2, \ldots, 8)$ denotes the electrical lengths of stubs.

For verification, we set reference frequency $f_0 = 2.5\,\text{GHz}$, $\theta_1 = \theta_3 = 15°$, $\theta_2 = 85°$, $\theta_4 = 65°$, $\theta_5 = 10°$, $\theta_6 = 30°$, $\theta_7 = 80°$, $\theta_8 = 50°$, $Y_1 = Y_2 = 2Y_3 = Y_4 = Y_8 = 1/100\,\text{S}$, $2Y_5 = 2Y_6 = Y_7 = 1/80\,\text{S}$. It should be known that the electrical lengths of all stubs are calculated at the reference frequency f_0. By solving Equations (1) and (3), it can be found that five transmission poles and three TZs are excited in the desired passband range.

Figure 2(a) shows the frequency responses of transmission coefficient $|S_{21}|$ and magnitude of Z_{in}, where Z_{in1}, Z_{in2}, and Z_{in3} represent the three input impedances enclosed by the orange rectangle box in Fig. 2(b). If the input impedance is zero at a certain frequency, the transmission signals will be blocked. And a TZ will be generated at this frequency. In this paper, these three TZs can be derived from the following equations:

$$Z_{\text{in1}} = j\frac{Z_6}{2} \frac{Z_6 \tan\theta_6 - Z_7 \cot\theta_7}{Z_6 + Z_7 \cot\theta_7 \tan\theta_6} \tag{7}$$

$$\begin{aligned} Z_{\text{in2}} &= \frac{Z_3}{2} \frac{-j\dfrac{Z_4 Z_5 \cot\theta_4 \cot\theta_5}{Z_4 \cot\theta_4 + Z_5 \cot\theta_5} + jZ_3 \tan\theta_3}{Z_3 + \dfrac{Z_4 Z_5 \cot\theta_4 \cot\theta_5 \tan\theta_3}{Z_4 \cot\theta_4 + Z_5 \cot\theta_5}} \\ &= j\frac{Z_3}{2} \frac{Z_3 Z_4 \tan\theta_3 \cot\theta_4 + Z_3 Z_5 \tan\theta_3 \cot\theta_5 - Z_4 Z_5 \cot\theta_4 \cot\theta_5}{Z_3 Z_4 \cot\theta_4 + Z_3 Z_5 \cot\theta_5 + Z_4 Z_5 \cot\theta_4 \cot\theta_5 \tan\theta_3} \end{aligned} \tag{8}$$

$$Z_{\text{in3}} = -jZ_8 \cot\theta_8 \tag{9}$$

As we can see in Fig. 2, $\text{TZ}_i\,(i = 1, 2, 3)$ in Fig. 2(a) corresponds to $Z_{\text{in}i}\,(i = 1, 2, 3)$ in Fig. 2(b). It agrees with the solution of Equations (7)–(9).

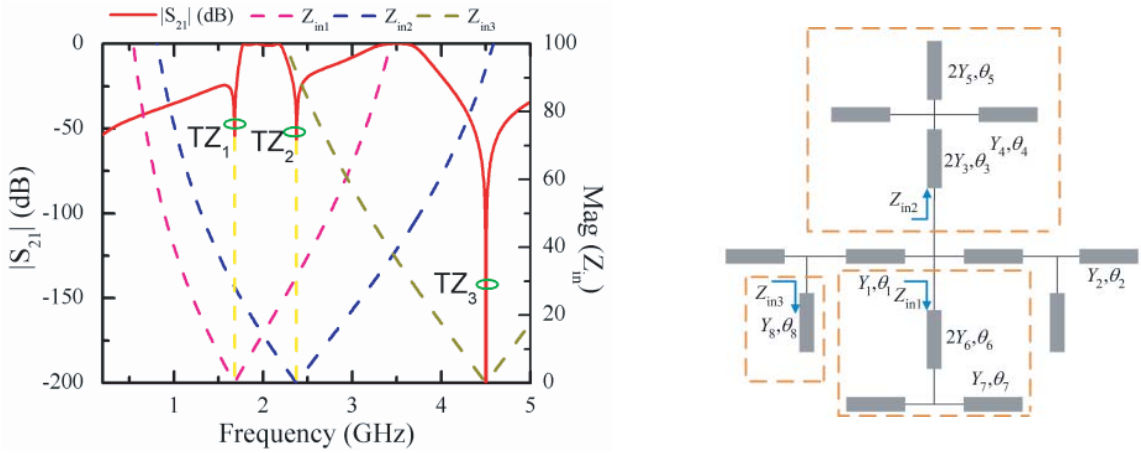

(a) (b)

Figure 2. (a) Frequency response of $|S_{21}|$ and Z_{in}, (b) ideal model circuit of the proposed resonator.

The variation of the TZs and transmission poles with θ_1, θ_3, θ_7, and θ_8 is illustrated in Fig. 3. It can be found that five transmission poles and three TZs have been excited, among which f_{o1} and f_{o2} represent the two odd-mode resonant frequencies, and f_{e1}, f_{e2} and f_{e3} represent the three even-mode resonant frequencies, while f_{z1}, f_{z2}, and f_{z3} represent the three TZs.

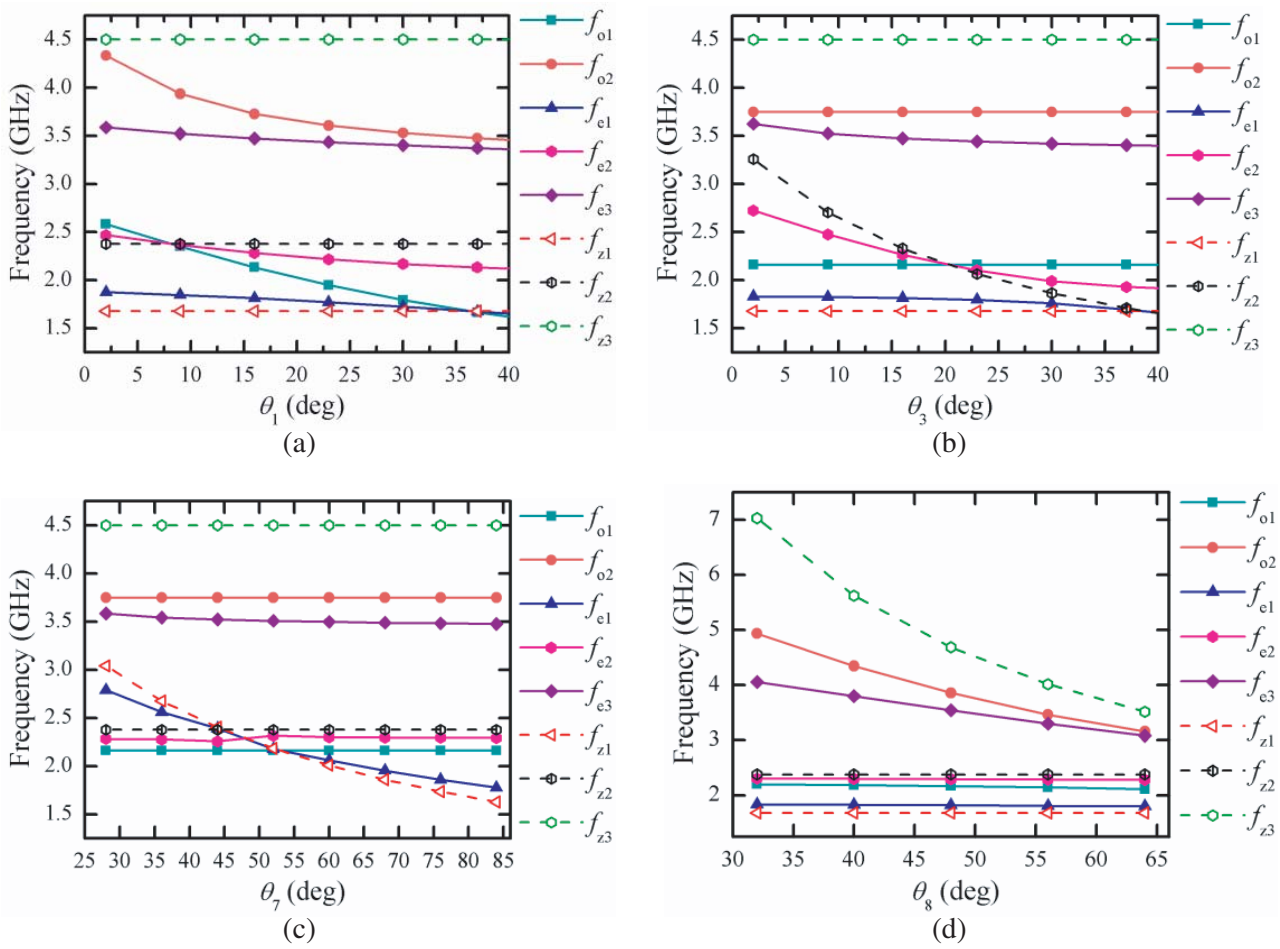

Figure 3. Variation of the resonant properties versus varied θ_i ($i = 1, 3, 7, 8$).

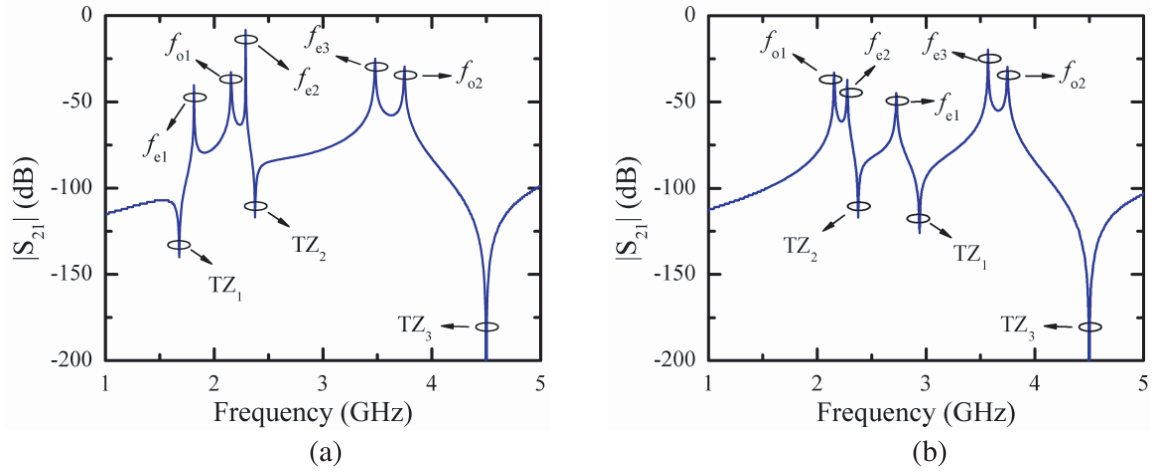

Figure 4. Frequency response of the QMR with weak coupling.

As shown in Fig. 3(a), f_{o1}, f_{o2}, f_{e2}, and f_{e3} decrease with the increase of θ_1, while other resonant frequencies are almost unchanged. In Fig. 3(b), θ_3 mainly affects f_{z2} and f_{e2}. Similarly, it can be seen that with the increase of θ_7, f_{e1} and f_{z1} gradually decrease, whereas other resonant frequencies and

TZs remain almost unchanged in Fig. 3(c). As depicted in Fig. 3(d), f_{o2}, f_{e3}, and f_{z3} decrease with the increase of θ_8, whereas f_{o1}, f_{e1}, f_{e2}, f_{z1}, f_{z2} keep constant.

According to Fig. 3(c), when $\theta_7 = 80°$, five transmission poles can be divided into two groups which meet the demand of realizing a dual-band BPF. And the frequency response with weak coupling is shown in Fig. 4(a). Moreover, according to Fig. 3(c), a tri-band BPF can be realized when $\theta_7 = 30°$. The simulation result of the frequency response of the proposed QMR with weak coupling is shown in Fig. 4(b). Therefore, different filters can be realized under the condition that the resonant frequencies are arranged in different groups by tuning the electrical lengths of the stubs properly.

3. DUAL-BAND BPF DESIGN

The key to generate a dual-band BPF is to divide the resonant modes into two groups by selecting the electrical lengths properly. According to Fig. 3(c), the demand of realizing a dual-band BPF can be met when $\theta_7 = 80°$. Under this case, $f_{z1} < f_{e1} < f_{o1} < f_{e2} < f_{z2} < f_{e3} < f_{o2} < f_{z3}$, namely, f_{o1}, f_{e1}, f_{e2} form the lower passband, and f_{o2}, f_{e3} form the higher passband. According to the analysis mentioned above, the corresponding physical dimensions can be calculated by using the impedance calculator.

Figure 5 depicts the frequency responses of $|S_{21}|$ versus varied L_7 and L_8. It can be seen in Fig. 5(a) that the variation of L_7 mainly influences BW of the first passband without affecting the second. In Fig. 5(b), the variation of L_8 mainly affects the second passband while the first passband keeps unchanged. Thus, the BWs of both passbands of the proposed dual-band BPF can be controlled independently.

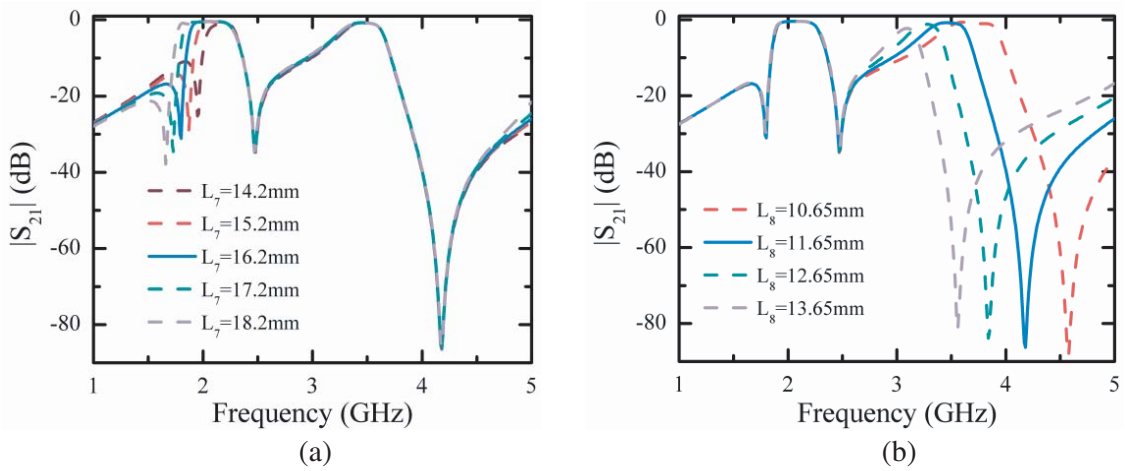

Figure 5. Transmission coefficient $|S_{21}|$ versus varied (a) L_7, (b) L_8.

Based on the analysis mentioned above, a dual-band BPF is fabricated on a substrate of Rogers 4003C with relative dielectric constant of 3.38, thickness of 0.508 mm, and loss tangent of 0.0027. The physical layout of the proposed dual-band BPF is shown in Fig. 6. After optimization in Sonnet 14.52, the final values of all the dimension parameters are given as follows (all in millimeter): $L_1 = 2.35$, $L_2 = 17.4$, $L_3 = 2.9$, $L_4 = 9$, $L_5 = 1.5$, $L_6 = 6.1$, $L_7 = 16.2$, $L_8 = 12.1$, $W_1 = W_2 = 0.225$, $W_3 = 0.2$, $W_4 = 0.25$, $W_5 = 0.35$, $W_6 = 0.5$, $W_7 = 0.4$, $W_8 = 0.2$, $fl = 12$, $fw = 0.25$, $S_1 = 0.125$, $S_2 = 0.2$. The filter is measured by an Agilent E5071C vector network analyzer. A photograph of the fabricated dual-band BPF is shown in Fig. 7(b). The overall circuit size of the BPF is 16.4 mm × 18.7 mm (excluding feeding lines), which corresponds to the size of $0.19\lambda_g \times 0.21\lambda_g$, where λ_g is the guided wavelength at 2.1 GHz. The simulated and measured results of the dual-band BPF are plotted in Fig. 7(a). The center frequencies of the two passbands are located at 2.1 GHz and 3.43 GHz, respectively. The minimum insertion losses of the two passbands are 1.4 and 1.9 dB. The out of band rejection at frequency of three TZs is higher than 25 dB. The measured return losses are better than 13 dB and 19 dB in the two passbands. Table 1 shows a performance comparison of this designed filter and some reported filters.

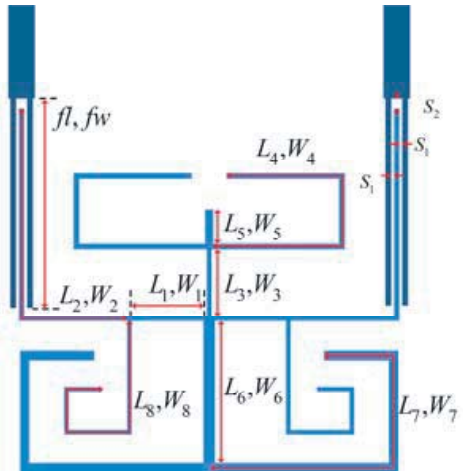

Figure 6. Physical layout of the proposed dual-band BPF.

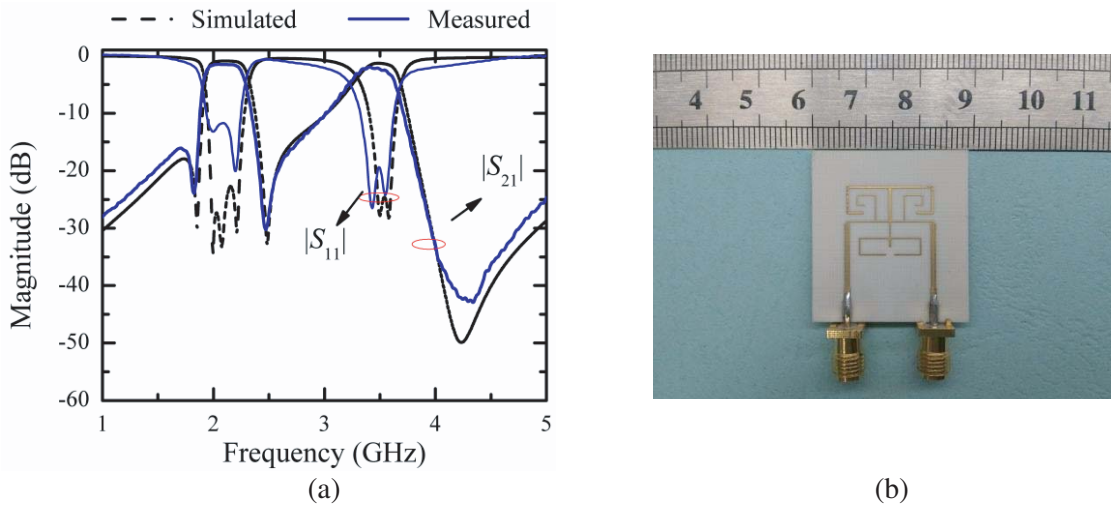

Figure 7. (a) Simulated and measured frequency responses of the dual-band BPF, (b) photograph of the fabricated dual-band BPF.

Table 1. Performance comparison with referenced works.

Ref.	Independently Controllable BW	Center frequency (GHz)	3 dB fractional bandwidth (%)	Insertion loss (dB)	Size ($\lambda_g \times \lambda_g$)
Filter B in [1]	Yes	2.4/5.8	4.63/3.6	1.35/1.97	0.39×0.25
[2]	Yes	2.77/3.55	3/4.7	5.2/4.9	0.3×0.3
[8]	No	2.45/5.2	18/4.8	0.6/0.9	0.11×0.23
Fig. 10 in [15]	No	2.4/5.8	8/5	1.1/2.2	0.68×0.158
This work	Yes	2.1/3.43	17.1/12.2	1.4/1.9	0.19×0.21

4. TRI-BAND BPF DESIGN

According to Fig. 3(c), when $\theta_7 = 30°$, $f_{o1} < f_{e2} < f_{z2} < f_{e1} < f_{z1} < f_{e3} < f_{o2} < f_{z3}$, five transmission poles are divided into three groups by three TZs. In order to improve the performance of the filter, the effect of L_i ($i = 4$, 8) on resonant frequencies is investigated, and the results are shown in Fig. 8. As shown in Fig. 8(a), f_{z2} decreases with the increase of L_4, and f_{e1} and f_{e2} decrease with the increase of L_4. Therefore, the BWs of the first and second passbands can be controlled by changing L_4. It can be seen in Fig. 8(b) that L_8 mainly affects f_{o2}, f_{e3}, and f_{z3}, while other resonant frequencies keep unchanged, which result in the BW change of the third passband. Thus, the tri-band BPF could be generated by selecting the electrical lengths of several stubs properly.

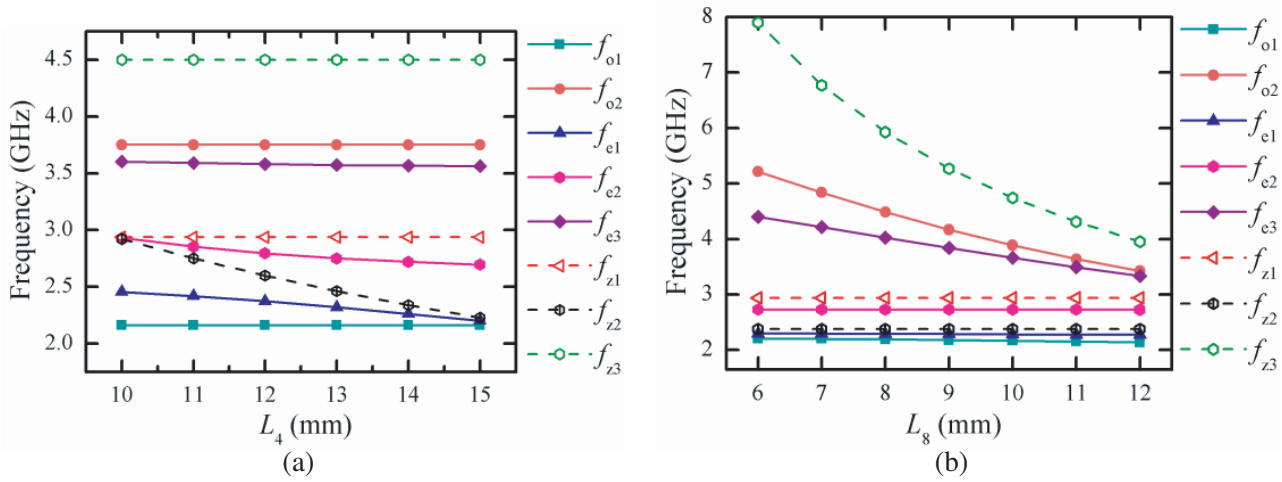

Figure 8. Variation of the resonant properties versus varied L_i ($i = 4$, 8).

According to the analysis above, tri-band BPF is fabricated on a substrate of Rogers 4003C with relative dielectric constant of 3.38, thickness of 0.508 mm, and loss tangent of 0.0027. The physical layout of the tri-band BPF is shown in Fig. 9. The values of parameters after optimization in Sonnet 14.52 are as follows (all in millimeter): $L_1 = 2.45$, $L_2 = 15.325$, $L_3 = 2.4$, $L_4 = 6.1$, $L_5 = 1.5$, $L_6 = 6.1$, $L_7 = 6$, $L_8 = 6.3$, $W_1 = W_2 = 0.225$, $W_3 = 0.2$, $W_4 = 0.25$, $W_5 = 0.35$, $W_6 = 0.3$, $W_7 = 0.4$, $W_8 = 0.45$, $S_1 = 0.125$, $S_2 = 0.2$, $fl = 9.925$, $fw = 0.25$. To investigate the performance, Agilent E5071C vector

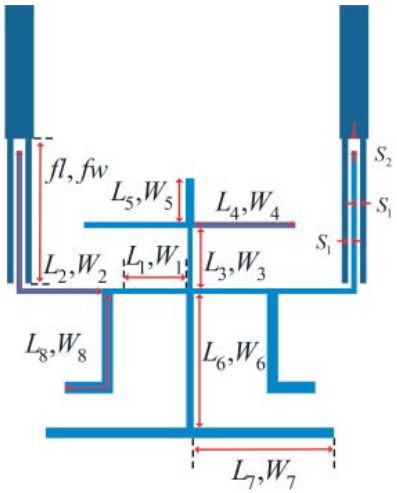

Figure 9. Physical layout of the proposed tri-band BPF.

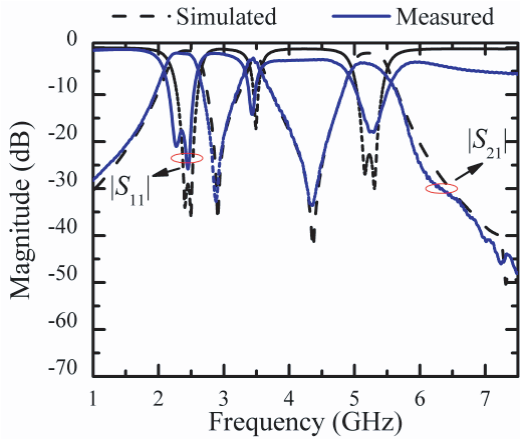

Figure 10. (a) Simulated and measured frequency responses of the tri-band BPF, (b) photograph of the fabricated tri-band BPF.

network analyzer is used to measure the S-parameter of the proposed filter. A photograph of the tri-band BPF is shown in Fig. 10(b). The overall size of the BPF is 16.9 mm × 16.65 mm (excluding feeding lines), which corresponds to the size of $0.22\lambda_g \times 0.21\lambda_g$, where λ_g is the guided wavelength at 2.35 GHz. The comparison between the simulated and the measured results is shown in Fig. 10(a). The center frequencies of these three passbands are 2.35 GHz, 3.44 GHz, and 5.2 GHz. The minimum insertion losses are 1.1, 2.2, and 3 dB. The out of band rejection at frequency of TZ is higher than 30 dB.

Furthermore, a performance comparison of this work and some reported works is shown in Table 2. It can be observed that the proposed QMR exhibits merits of compact size, wide fractional bandwidth, and flexible design.

Table 2. Performance comparison with referenced works.

Ref.	Two filters based on the same topology	Center frequency (GHz)	3 dB fractional bandwidth (%)	Insertion loss (dB)	Size ($\lambda_g \times \lambda_g$)
[3]	No	1.575/2.4/3.5	5.3/3.8/4.6	1.6/1.5/2.3	0.358 × 0.405
[4]	No	1.8/3.5/5.8	7/5/3.5	0.88/1.33/ 1.77	0.108 × 0.521
[6]	Yes	2.5/3.68/5.04	16.7/14.4/ 13.2	0.24/0.33/0.4	0.31 × 0.32
Fig. 12 in [12]	No	2.35/4.78/7.21	5.31/6.27/ 8.66	1.78/0.9/0.7	0.311 × 0.311
This work	Yes	2.35/3.44/5.2	20.8/7.7/ 11.15	1.1/2.2/3	0.22 × 0.21

5. CONCLUSION

In this paper, a dual-band BPF and a tri-band BPF based on the same topology are presented. The resonant modes and TZs of the filters can be easily adjusted by changing the electrical lengths of certain stubs. The BWs of the proposed filters are controllable. And the BWs of dual-band BPF can be controlled independently. The measured results agree well with the simulated ones. Moreover, the location of the passband and flexible design make the filters attractive in the wireless communication system.

REFERENCES

1. Zhang, Z. C., Q. X. Chu, and F. C. Chen, "Compact dual-band bandpass filters using open-/short-circuited stub-loaded $\lambda/4$ resonator," *IEEE Microwave and Wireless Components Letters*, Vol. 25, No. 10, 657–659, 2015.
2. Lin, F., Q. X. Chu, and S. W. Wong, "Design of dual-band filtering quadrature coupler using $\lambda/2$ and $\lambda/4$ resonators," *IEEE Microwave and Wireless Components Letters*, Vol. 22, No. 11, 565567, 2012.
3. Chen, W. Y., M. H. Weng, and S. J. Chang, "A new tri-band bandpass filter based on stub-loaded step-impedance resonator," *IEEE Microwave and Wireless Components Letters*, Vol. 22, No. 4, 179–181, 2012.
4. Zhang, S. B. and L. Zhu, "Compact tri-band bandpass filter based on $\lambda/4$ resonators with Ufolded coupled-line," *IEEE Microwave and Wireless Components Letters*, Vol. 23, No. 5, 258–260, 2013.
5. Ghatak, R., M. Pal, P. Sarkar, and D. R. Poddar, "Dual-band bandpass filter using integrated open loop resonators with embedded ground slots," *Microwave and Optical Technology Letters*, Vol. 54, No. 9, 2049–2052, 2012.
6. Wang, Z. J., C. Wang, and N. Y. Kim, "Dual-/triple-wideband microstrip bandpass filter using independent triple-mode stub-loaded resonator," *Microwave and Optical Technology Letters*, Vol. 60, No. 1, 56–64, 2018.
7. Hsu, C. Y., C. Y. Chen, and H. R. Chuang, "A miniaturized dual-band bandpass filter using embedded resonators," *IEEE Microwave and Wireless Components Letters*, Vol. 21, No. 12, 658–660, 2011.
8. Liu, H. W., B. P. Ren, X. H. Guan, J. H. Lei, and S. Li, "Compact dual-band bandpass filter using quadruple-mode square ring loaded resonator (SRLR)," *IEEE Microwave and Wireless Components Letters*, Vol. 23, No. 4, 181–183, 2013.
9. Gao, L. and X. Y. Zhang, "High-selectivity dual-band bandpass filter using a quad-mode resonator with source-load coupling," *IEEE Microwave and Wireless Components Letters*, Vol. 23, No. 9, 474–476, 2013.
10. Gao, L., X. Y. Zhang, and Q. Xue, "Compact tri-band bandpass filter using novel eight-mode resonator for 5G WiFi application," *IEEE Microwave and Wireless Components Letters*, Vol. 25, No. 10, 660–662, 2015.
11. Liu, H. W., Y. Wang, X. M. Wang, J. H. Lei, W. Y. Xu, Y. L. Zhao, B. P. Ren, and X. H. Guan, "Compact and high selectivity tri-band bandpass filter using multimode stepped-impedance resonator," *IEEE Microwave and Wireless Components Letters*, Vol. 23, No. 10, 536–538, 2013.
12. Luo, S., L. Zhu, and S. Sun, "Compact dual-mode triple-band bandpass filters using three pairs of degenerate modes in a ring resonator," *IEEE Transactions on Microwave Theory and Techniques*, Vol. 55, No. 5, 1222–1229, 2011.
13. Li, J., S. S. Huang, H. Wang, Y. Li, and J. Z. Zhao, "A novel compact triband bandpass filter using SIR embedded quarter-wavelength resonators," *Microwave and Optical Technology Letters*, Vol. 57, No. 6, 1345–1349, 2015.
14. Majidifar, S. and M. Hayati, "New approach to design a compact triband bandpass filter using a multilayer structure," *Turkish Journal of Electrical Engineering & Computer Sciences*, Vol. 25, 4006–4012, 2017.
15. Zhang, S. B. and L. Zhu, "Synthesis design of dual-band bandpass filters with $\lambda/4$ stepped-impedance resonators," *IEEE Transactions on Microwave Theory and Techniques*, Vol. 61, No. 5, 1812–1819, 2013.